IOP Publishing Journal of Physics: Condensed Matter
J. Phys.: Condens. Matter **30** (2018) 435305 (7pp) https://doi.org/10.1088/1361-648X/aae3b9

The effect of structural asymmetry on thermal rectification in nanostructures

Xueming Yang[1,2], Jiangxin Xu[1], Sihan Wu[1], Dapeng Yu[1] and Bingyang Cao[2]

[1] Department of Power Engineering, North China Electric Power University, Baoding 071003, People's Republic of China
[2] Key Laboratory for Thermal Science and Power Engineering of Ministry of Education, Department of Engineering Mechanics, Tsinghua University, Beijing 100084, People's Republic of China

E-mail: ncepub@hotmail.com (X Yang) and caoby@tsinghua.edu.cn (B Cao)

Received 21 March 2018, revised 25 August 2018
Accepted for publication 24 September 2018
Published 9 October 2018

Abstract

Three SWCNT-graphene nanostructure-based models are designed to probe the thermal rectification caused by the structural asymmetry in the boundary thermal contacts, the device, and the whole system, respectively. We find that both the asymmetry of entire system and the asymmetry of the device are not necessary condition for the existence of thermal rectification, and the asymmetry in boundary thermal contacts is more important than the asymmetry in device toward determining both the magnitude and the direction of thermal rectification. Interestingly, notable thermal rectification can exist in the systems with overall structural symmetry when the boundary thermal contacts are structurally asymmetric. Moreover, nanostructures with a structurally symmetric device and structurally asymmetric boundary thermal contacts can still display significant thermal rectification. These findings could offer insight into the future design and performance improvement of nanostructured thermal rectifiers.

Keywords: structural asymmetry, thermal rectification, carbon nanotube-graphene nanostructures, resonance, standing wave, molecular dynamics

(Some figures may appear in colour only in the online journal)

Nomenclature

J_+	Heat current corresponds to $\Delta > 0$, μW
J_-	Heat current corresponds to $\Delta < 0$, μW
S_+	Overlap of the power spectra corresponds to $\Delta > 0$, dimensionless
S_-	Overlap of the power spectra corresponds to $\Delta < 0$, dimensionless
T_0	Average temperature, K
E_{hot}	Total energy acquired from the atoms in the hot thermostats, μJ
E_{cold}	Total energy lost from the atoms in the cold thermostats, μJ
δ_{F}	Thickness of the fixed part, angstrom
L_{C}	Carbon nanotube length, angstrom
L_{GR}	Side length of the right graphene sheet after excluding the fixed part, angstrom
L_{GL}	Side length of the left graphene sheet after excluding the fixed part, angstrom
δ_{T}	Thickness of the square ring heating bath region, angstrom
$P_{\mathrm{w}}(\omega)$	Power spectrum of the wide sides of the device
$P_{\mathrm{n}}(\omega)$	Power spectrum of the narrow sides of the device

Greek symbols

Δ	Normalized temperature difference, dimensionless
η	Thermal rectification ratio, dimensionless
$\eta_{\max}$	Maximum thermal rectification ratio, dimensionless

 © 2018 IOP Publishing Ltd Printed in the UK

1. Introduction

As the counterpart of an electronic rectifier, a thermal rectifier or thermal diode is a device which allows heat to flow preferentially in one direction while restricting it in the opposite direction [1, 2]. Due to its great potential for applications in the field of thermal management and phononics applications [3–6], substantial attention has been paid to exploring new nanostructures with thermal rectification and to the study of novel thermal rectification mechanism [7–29]. Many studies have reported the thermal rectification in nanostructures with asymmetric shapes [18–29]. To understand the role that shape asymmetry played in thermal rectification, Lee *et al* [23] investigated thermal rectification in 3D asymmetric nanostructures. In their study, a thermal rectification system (excluding the fixed part) is divided into two parts: the thermostated parts are considered as the boundary thermal contacts, and the free part of the system considered as the device. The two parts are seamlessly conjoined by covalent bonds and in the same crystalline material. Their study shows that size asymmetry in the boundary thermal contacts has a significant effect on thermal rectification. Additionally, Gordiz *et al* [30] investigated the thermal rectification in multi-walled carbon nanotube, and they found that asymmetric thermal reservoirs can produce the thermal rectification when the device is also asymmetric. Recently, Ming *et al* [31] further investigated the influence of the nonlinear system-bath coupling and the boundary effect in thermal rectification in harmonic chains.

In this study, we focus on the effect of structural asymmetry on thermal rectification. It should be emphasized that, for a structurally symmetric nanostructure, both the lattice structure and shape are symmetrical to the symmetrical axis of the overall structure along the direction of the thermal rectification. In the following text, all terms of asymmetry and symmetry only refer to this structural asymmetry and structural symmetry.

In fact, the impact of asymmetry for both the boundary thermal contacts and the device on the thermal rectification of the overall system remains unclear. For example, it is still unknown whether thermal rectification can exist in a system with a symmetric device and asymmetric boundary thermal contacts and whether a system that satisfies overall system symmetry with asymmetric boundary thermal contacts can display thermal rectification. We will address these questions in this report. More importantly, to enable rational design of a more efficient thermal rectifier with asymmetric nanostructures, a fundamental and comprehensive understanding of the effect of structural asymmetry on thermal rectification is essential.

2. Models and methodology

We explore these questions based on several SWCNT-graphene junctions-based nanostructures. We examine the thermal rectification of three different models based on carbon nanotube-graphene junctions: Model A, Model B, and Model C, as shown in figure 1. Following the idea of Lee [23], the three models are divided into the fixed region, the boundary thermal contacts region, and the device region. It can be seen in figure 1 that the division of the device region (cyan) and the boundary thermal contacts region (red) in the three models is different. The edge parts (green) of the square graphene sheets at both ends are fixed, the thickness $\delta_F = 0.4\,\text{nm}$, the carbon nanotube length $L_C = 9.5\,\text{nm}$, and the side lengths of the right and left graphene sheets after excluding the fixed part are L_{GR} and L_{GL}, respectively. In the process of simulation, $L_{GR} = 2.8\,\text{nm}$ is fixed and L_{GL} varies from 2.8 nm to 12.8 nm. In Model B and Model C, the thickness of the square ring heating bath region $\delta_T = 0.4\,\text{nm}$.

The differences in symmetry of the three model structures should be noted. Model A: the device region is symmetric, but the boundary thermal contacts region is asymmetric when $L_{GL} > 2.8\,\text{nm}$. Model B: when $L_{GL} > 2.8\,\text{nm}$, both the device region and boundary thermal contacts region are asymmetric and the device region integrally shows the left end is wide and the right end is narrow. Model C: when $L_{GL} > 2.8\,\text{nm}$, both the device region and boundary thermal contacts are asymmetric; however, the device region integrally shows the right end is wide and the left end is narrow, which is in contrast to Model B. To facilitate the analysis and discussion in our simulations, the left end and right ends of the system are referred to as the wide end and narrow end, respectively.

Nonequilibrium molecular dynamics (NEMD) simulations are carried out for thermal rectification calculations using the large-scale atomic/molecular massively parallel simulator (LAMMPS) software package [32], and the optimized Tersoff potential [33] is adopted. The time step is set to 0.4 fs. In all the simulations, the atoms at the two sides colored in green in the model are fixed to make a suspended structure, and the free boundary condition is applied to all the directions. The system is relaxed in the NVT ensemble at $T_0 = 300\,\text{K}$ for 5×10^6 time steps using a Nose–Hoover thermostat. Following the suggestion of Wang [24], a Berendsen thermostat is then adopted for the boundary thermal contacts region. To establish a temperature gradient along the longitudinal direction of the tube, the system is performed for another 12×10^6 time steps under NVE ensemble. The temperatures in the heating bath zones of the wide and narrow ends are set to $T_0(1+\Delta)$ and $T_0(1-\Delta)$, respectively, where Δ represent the normalized temperature difference and the wide end is the hot end when $\Delta > 0$ and the narrow end is the hot end when $\Delta < 0$.

The thermal rectification ratio and the net heat flux are defined as

$$\eta = \frac{(J_+ - J_-)}{J_-} \times 100\%, \tag{1}$$

where J_+ and J_- represent the heat flux in the case of $\Delta > 0$ and $\Delta > 0$, respectively; $J_\pm = (\partial E_{hot}/\partial t + \partial E_{cold}/\partial t)/2$; E_{hot} and E_{cold} are the energy acquired/lost from the hot/cold end, respectively.

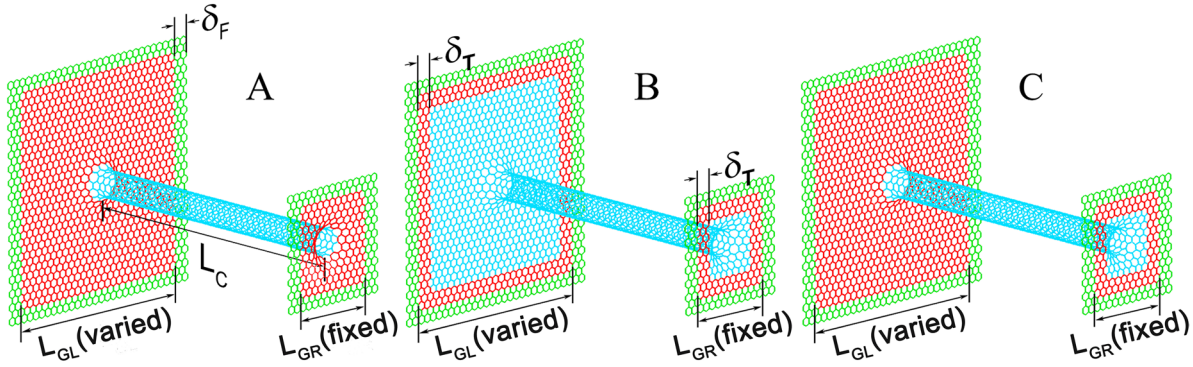

Figure 1. The schematic diagram of 3 CNT-graphene junction based models, Model A, Model B, and Model C, for calculating the thermal rectification. The green, red, and cyan regions represent the fixed part, the thermostated part, and the free part of the system, respectively.

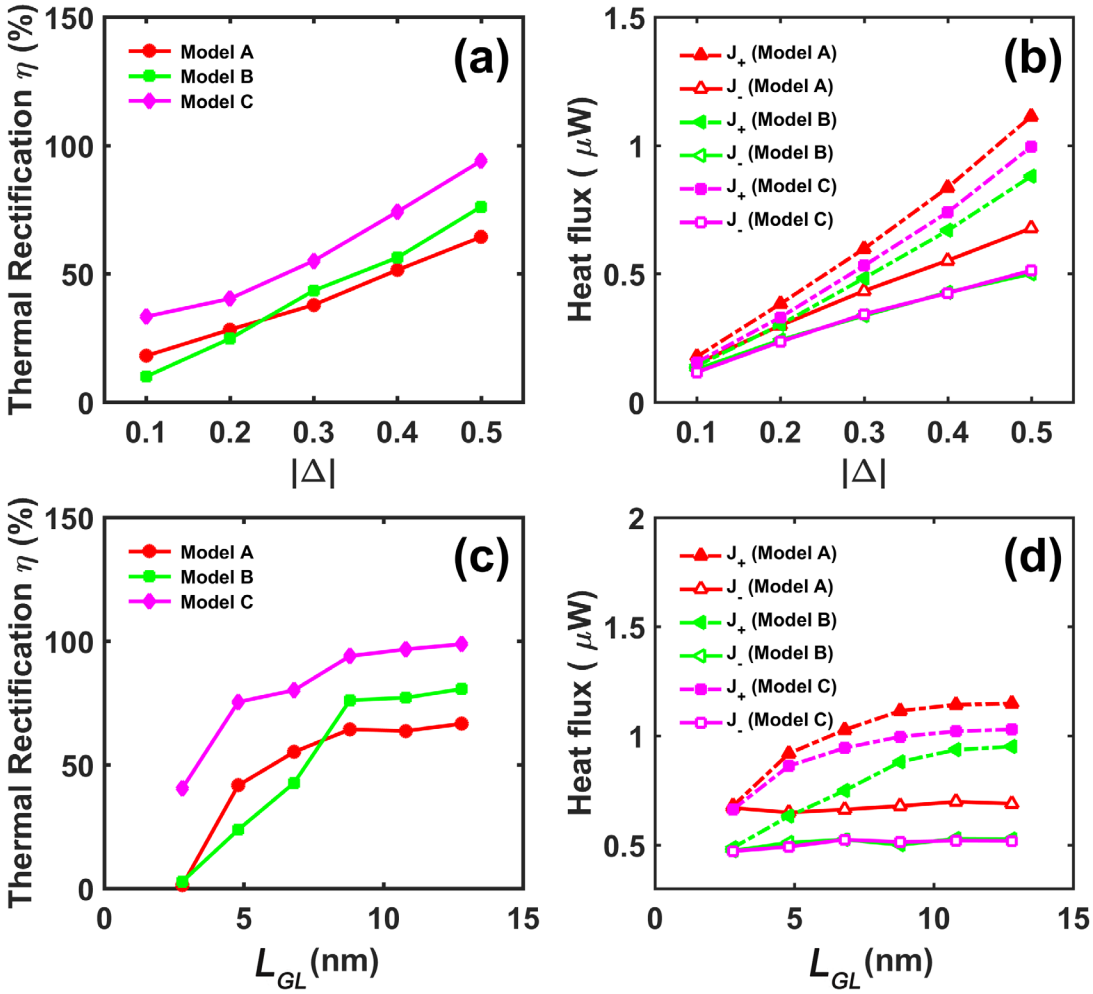

Figure 2. The thermal rectification results of Model A (triangle), Model B (square), and Model C (diamond). (a) and (b) Thermal rectification ratio and corresponding heat flux versus $|\Delta|$; (c) and (d) thermal rectification ratio and corresponding heat flux versus L_{GL}.

3. Results and discussion

The relationship of the calculated thermal rectification ratios of Model A, Model B, and Model C with L_{GL} and $|\Delta|$ and the relationship of the corresponding $J_{+}(J_{-})$ with L_{GL} and $|\Delta|$ are illustrated in figure 2. Figures 2(a) and (b) show the changes of the thermal rectification ratios of the three models ($L_{\mathrm{GL}} = 8.8\,\mathrm{nm}$) and the changes of heat flux, respectively, when the average temperature is 300 K and the values of $|\Delta|$ are increased from 0.1 to 0.5. The thermal rectification ratios of the three models and the heat flux increased almost linearly with $|\Delta|$. The thermal rectification ratios (η) of Model A, Model B, and Model C are 64.31% and 76.11% and 92.54% at $T = 300\,\mathrm{K}$ and $|\Delta| = 0.5$, respectively.

Figures 2(c) and (d) show the changes of the thermal rectification ratios for the three models ($|\Delta| = 0.5$) and the changes of heat flux under different L_{GL}, respectively. As the values of L_{GL} increased from 2.8 nm to 12.8 nm, the thermal rectification

ratios of each model (η) first increases sharply initially with increasing L_{GL}, and then it tends to converge to a constant value at approximately 8.8 nm, The maximum thermal rectification ratios (η_{max}) of Model A, Model B, and Model C are 66.6%, 80.6%, and 98.8%, respectively, corresponding to the L_{GL} value of 12.8 nm. For Model A, we can note that the device region is symmetric but the boundary thermal contacts and the entire system is asymmetric when $L_{GL} > 2.8$ nm, and the system has a significant thermal rectification effect. Therefore, we can conclude that the asymmetry of the device region is not a necessary condition for the existence of a thermal rectification effect and when the device is symmetric and the boundary thermal contacts is asymmetric the thermal rectification effect of the system can still be evident.

When $L_{GL} = L_{GR} = 2.8$ nm, it is important to note that the device region and the boundary thermal contacts region of Model A and Model B become both bilaterally symmetrical structures. As such, there is no thermal rectification effect, and the thermal rectification ratios basically equal zero. However, for Model C, although the entire system is bilaterally symmetrical, from the perspective of the size of the device region, the left end is narrow and the right end is wide, while from the perspective of the size of the boundary thermal contacts region, the left end is wide and the right end is narrow. Interestingly, we found that notable thermal rectification display in Model C. The calculated thermal rectification ratio of Model C is 40.5% when $L_{GL} = L_{GR} = 2.8$ nm, and this means that the heat flows easily from the left to right, and this is consistent with the asymmetric direction of the boundary thermal contacts region. The above analysis suggests that the asymmetry of the entire system is not a necessary condition for the existence of a thermal rectification effect. When the system has an overall structure that is symmetric and a boundary thermal contacts region that is asymmetric, it can still exhibit a thermal rectification effect. This also indicated that the asymmetry in boundary thermal contacts is more important than the asymmetry in device toward determining both the magnitude and the direction of thermal rectification.

In order to analyze the underlying mechanism of the thermal rectification effect in each model, we calculate the power spectra. The power spectrum is considered a good qualitative and quantitative method to explain the thermal rectification effect. For the above three models ($L_{GL} = 8.8$ nm, $|\Delta| = 0.5$), in the vibration density of states (vDOS) calculation, we choose the atoms of the device in the first two unit cells away from each thermal contact region. The results are shown in figure 3: the power spectra of the wide and narrow ends of the three models overlap relatively well when $\Delta = 0.5$; however, when $\Delta = -0.5$, an obvious mismatch in the power spectra of the wide and narrow ends of each model can be observed, with significant low-frequency peaks appearing at 1.34 THz in each model. The power spectra of the three models show obvious mismatches under negative thermal bias.

The match/mismatch of the vDOS is considered an important mechanism of thermal rectification [34]. To quantify the analysis of the match or mismatch of the vDOS, the overlaps (S) of the vDOS are calculated as follows:

$$S_{\pm} = \frac{\int P_w(\omega) \cdot P_n(\omega) d\omega}{\left(\int P_w(\omega)^2 d\omega\right)^{1/2} \cdot \left(\int P_n(\omega)^2 d\omega\right)^{1/2}} \quad (2)$$

where S_+ and S_- are the overlaps of the vDOS in the case of $\Delta > 0$ and $\Delta < 0$, respectively; $P_w(\omega)$ is the power spectrum of the wide end of the device; and $P_n(\omega)$ is the power spectrum of the narrow end of the device.

The value of S_+/S_- is generally used to assess the degree of mismatch of the power spectrum, and the larger the value, the higher the degree of mismatch. The calculated results show that the S_+ of Model A, Model B, and Model C are 0.9789, 0.8843, and 0.8939, respectively; S_- of Model A, Model B, and Model C are 0.8724, 0.6376, and 0.4873, respectively; and S_+/S_- of Model A, Model B, and Model C are 1.122, 1.3869, and 1.8344, respectively. The values of S_+/S_- match with the thermal rectification ratio of each model; namely, the thermal rectification ratio of Model C is the largest, Model B is the second largest, and Model A is the smallest. Therefore, the thermal rectification effect is reasonably explained by the mismatch in the power spectra of the wide and narrow ends under negative thermal bias.

To understand why notable thermal rectification exhibit in Model C when the entire system is symmetric, we calculated the S_+/S_- of Model A, Model B, and Model C in the case of $L_{GL} = L_{GR} = 2.8$ nm ($|\Delta| = 0.5$). The calculated values of S_+/S_- of Model A, Model B, and Model C are 1.004, 1.027, and 1.136, respectively. Considering $\eta = (J_+ - J_-)/J_- \sim (S_+/S_-)^{\delta_R} - 1$ ($\delta_R = 1.68 \pm 0.08$) [34, 35], we can obtain that thermal rectification ratio in this case for Model A, Model B is basically equal zero, but is notable for Model C.

To confirm whether the significant low-frequency peak appearing in vDOS is related to the standing wave under the negative thermal bias, the velocity autocorrelation function (VACF) of the groups of atoms in the vDOS regions for the three models is calculated. In fact, the periodic components in VACF correspond to the periodic component of its original signal. As shown in figures 4(a), (c) and (e), when $\Delta = -0.5$, the VACF for Model A has some noise but still shows obvious periodicity, and the periodicity of the VACF for Model B and Model C are more obvious and dominate the vibration. The periodicity in the VACF indicates the standing waves existed in original signal. As can be seen from the figure, the frequencies of the standing waves in Model A, Model B, and Model C are all 1.34 THz, and this is consistent with the results from the vDOS calculations. Figures 4(b), (d) and (f) show the results of VACF calculations for Model A, Model B, and Model C at $\Delta = 0.5$, respectively, and the amplitude of the VACF rapidly decay and have no obvious periodicity. The above results suggest that there are obvious standing waves at the narrow ends under the negative thermal bias and that the existence of standing waves greatly hinders the transfer of thermal energy. This is why the heat flux under the negative thermal bias is obviously less than under the positive thermal bias.

We also calculate the natural frequencies of the narrow end of the device for Model A, Model B, and Model C. As shown in figure 5, the natural frequencies of 1.34 THz

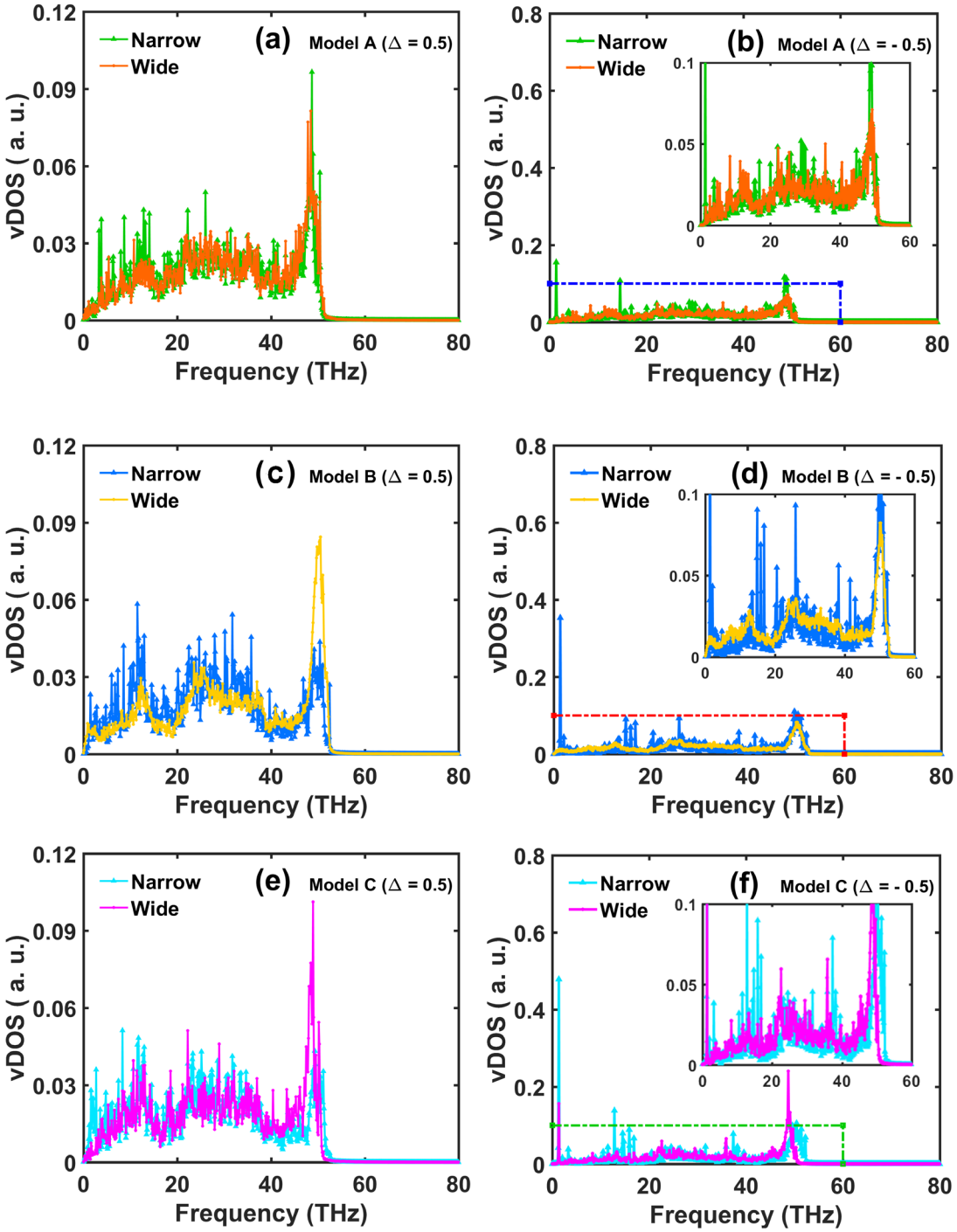

Figure 3. vDOS per atom for Model A, Model B, and Model C. (a) and (b): Model A; (c) and (d): Model B; (e) and (f): Model C.

coincide with the significant low-frequency peaks of 1.34 THz in the VDOS as shown in figures 3(b), (d), and (f), indicating that the standing wave that exists at the narrow end under negative thermal bias is actually a resonance at the natural frequency of 1.34 THz. In fact, the thermal conductivity reduction by local resonance in nanostructures has been found and reported [36–38]. Additionally, Li *et al* [34] has reported that the resonance effect in the temperature-dependent power spectrum versus frequency as a result of the nonlinear lattice dynamics is one of the important underlying physical mechanisms of the thermal rectification. In this study, the resonances that appear at the narrow end of the models under negative thermal bias heavily block phonon transport thus lead to much lower thermal conductivity than those under positive thermal bias, which explain the thermal rectification effect.

Our above study is based on the idea of Lee that the thermal contacts is considered as the part of the system; however one might argue that the exclusion of thermal reservoirs from the system of interest, as adopted in many NEMD studies, is the way to study the intrinsic material property of the device. In the opinion of the latter, the system only means the device. If this view is correct, we can draw some more interesting conclusions: (1) a structural symmetry system can have thermal

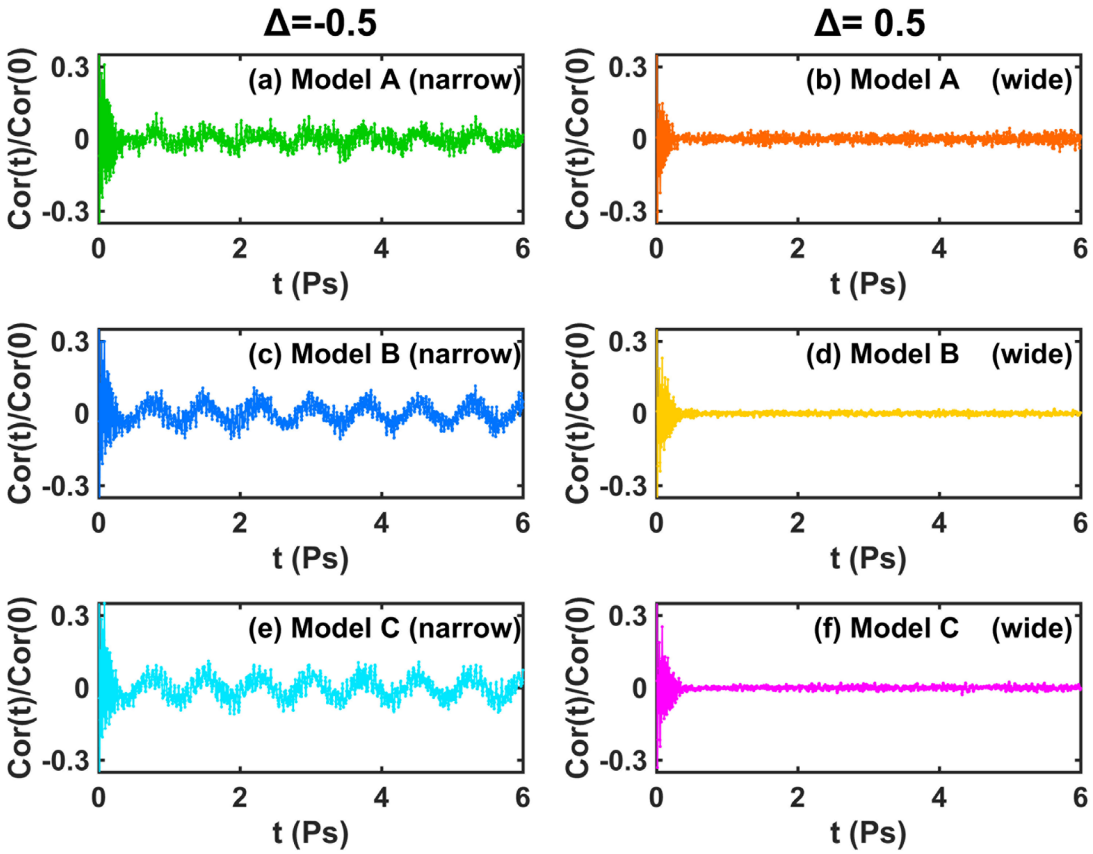

Figure 4. The VACF calculation of Model A, Model B, and Model C. (a) and (b): Model A; (c) and (d): Model B; (e) and (f): Model C.

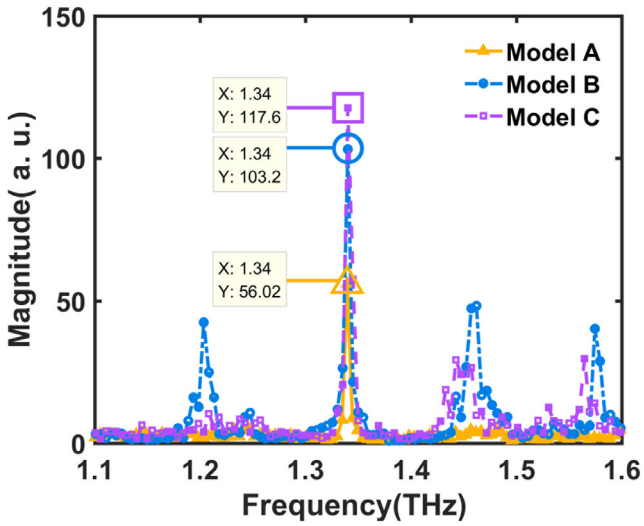

Figure 5. The calculated natural frequencies for Model A, Model B, and Model C.

rectification when an asymmetry thermal reservoir is applied; (2) the direction of a thermal rectifier can be changed by applying reversed asymmetry thermal reservoir.

4. Conclusions

In summary, the thermal rectification of the three different models of CNT-graphene nanostructures are investigated using NEMD simulations, and the impact of asymmetry in the boundary thermal contacts region and device asymmetry on the thermal rectification of the overall system is analyzed and explored. We found that both the asymmetry of entire system and the asymmetry of the device are not necessary condition for the existence of thermal rectification, and the asymmetry in boundary thermal contacts is more important than the asymmetry in device toward determining both the magnitude and the direction of thermal rectification. Notable thermal rectification can exist in the systems with overall structural symmetry when the boundary thermal contacts are structurally asymmetric. Moreover, nanostructures with a structurally symmetric device and structurally asymmetric boundary thermal contacts can still display significant thermal rectification. These findings could offer important implications for future design and performance improvement of nanostructured thermal rectifiers.

Acknowledgments

This research is supported by the National Natural Science Foundation of China (Grant No. 51576066), the Natural Science Foundation of Hebei Province of China (Grant No. E2014502042).

Conflicts of interest

The authors declare no competing financial interests.

ORCID iDs

Xueming Yang https://orcid.org/0000-0001-7309-7817

References

[1] Li B, Wang L and Casati G 2004 *Phys. Rev. Lett.* **93** 184301
[2] Chang C W, Okawa D, Majumdar A and Zettl A 2006 *Science* **314** 1121
[3] Martínez-Pérez M J, Fornieri A and Giazotto F 2015 *Nat. Nanotechnol.* **10** 303
[4] Casati G 2007 *Nat. Nanotechnol.* **2** 23
[5] Wang L and Li B 2007 *Phys. Rev. Lett.* **99** 177208
[6] Wang L and Li B 2008 *Phys. Rev. Lett.* **101** 267203
[7] Rurali R, Cartoixà X and Colombo L 2014 *Phys. Rev.* B **90** 041408
[8] Pei Q X, Zhang Y W, Sha Z D and Shenoy V B 2012 *Appl. Phys. Lett.* **100** 101901
[9] Chen X K, Hu J W, Wu X J, Jia P, Peng Z H and Chen K Q 2018 *J. Phys. D: Appl. Phys.* **51** 085103
[10] Shih T M, Gao Z, Guo Z, Merlitz H, Pagni P J and Chen Z 2015 *Sci. Rep.* **5** 12677
[11] Zhao W, Wang Y, Wu Z, Wang W, Bi K, Liang Z, Yang J, Chen Y, Xu Z and Ni Z 2015 *Sci. Rep.* **5** 11962
[12] Chen X K, Xie Z X, Zhou W X, Tang L M and Chen K Q 2016 *Carbon* **100** 492
[13] Arora A, Hori T, Shiga T and Shiomi J 2017 *Phys. Rev.* B **96** 165419
[14] Zhang T and Luo T 2015 *Small* **11** 4657
[15] Zhu J, Hippalgaonkar K, Shen S, Wang K, Abate Y, Lee S, Wu J, Yin X, Majumdar A and Zhang X 2014 *Nano Lett.* **14** 4867
[16] Ito K, Nishikawa K, Iizuka H and Toshiyoshi H 2014 *Appl. Phys. Lett.* **105** 253503
[17] Chen C *et al* 2015 *Sci. Rep.* **5** 8884
[18] Zhang G and Zhang H 2011 *Nanoscale* **3** 4604–7
[19] Noya E G, Srivastava D and Menon M 2009 *Phys. Rev.* B **79** 115432
[20] Yang X, Yu D and Cao B 2017 *ACS Appl. Mater. Interfaces* **9** 24078
[21] Yang X, Yu D, Cao B and To A C 2016 *ACS Appl. Mater. Interfaces* **9** 29
[22] Hu J, Ruan X and Chen Y P 2009 *Nano Lett.* **9** 2730
[23] Lee J, Varshney V, Roy A K, Ferguson J B and Farmer B L 2012 *Nano Lett.* **12** 3491
[24] Wang Y, Vallabhaneni A, Hu J, Qiu B, Chen Y P and Ruan X 2014 *Nano Lett.* **14** 592
[25] Cartoixà X, Colombo L and Rurali R 2015 *Nano Lett.* **15** 8255
[26] Liu Y Y, Zhou W X and Chen K Q 2015 *Sci. Rep.* **5** 17525
[27] Liu Y Y, Zhou W X, Tang L M and Chen K Q 2014 *Appl. Phys. Lett.* **105** 203111
[28] Zhang Z, Chen Y, Xie Y and Zhang S 2016 *Appl. Therm. Eng.* **102** 1075
[29] Yang N, Zhang G and Li B 2008 *Appl. Phys. Lett.* **93** 243111
[30] Gordiz K, Vaez Allaei S M and Kowsary F 2011 *Appl. Phys. Lett.* **99** 251901
[31] Ming Y, Li H M and Ding Z J 2016 *Phys. Rev.* E **93** 032127
[32] Plimpton S 1995 *J. Comput. Phys.* **117** 1
[33] Lindsay L and Broido D A 2010 *Phys. Rev.* B **81** 205441
[34] Li N, Ren J, Wang L, Zhang G, Hänggi P and Li B 2012 *Rev. Mod. Phys.* **84** 1045
[35] Li B, Lan J and Wang L 2005 *Phys. Rev. Lett.* **95** 104302
[36] Chen J, Zhang G and Li B 2011 *J. Chem. Phys.* **135** 104508
[37] Davis B L and Hussein M I 2014 *Phys. Rev. Lett.* **112** 055505
[38] Xiong S, Sääskilahti K, Kosevich Y A, Han H, Donadio D and Volz S 2016 *Phys. Rev. Lett.* **117** 025503